E De La Luna et al.

Recent results on high-triangularity H-mode studies in JET-ILW

Recent Results on High-Triangularity H-mode Studies in JET-ILW

E. de la Luna[1], F. Rimini[2] , P. Lomas[2], A. C. C. Sips[3], L. Frassinetti[4], P. Drewelow[5], J. Flanagan[2], B. Lomanowski[6], I. Nunes[7], A. Meigs[2] and JET contributors*

EUROFusion Consortium, JET, Culham Science Centre, Abingdon, OX14 3DB, UK
[1] Laboratorio Nacional de Fusión, CIEMAT, 28040, Madrid, Spain
[2] UKAEA, Culham Science Centre, Abingdon, OX14 3DB, UK.
[3] European Commission, B-1049 Brussels, Belgium
[4] VTT Technical Research Centre of Finland, P.O.Box 1000, FIN-02044 VTT, Finland
[5] Max-Planck-Institut für Plasmaphysik, 85748 Garching, Germany
[6] Centre for Advanced Instrumentation, Department of Physics, Durham University, UK
[7] IST, Instituto de Plasmas e Fusão Nuclear, Av Rovisco Pais, 1049-001, Lisbon, Portugal
*See the Appendix of F. Romanelli et al., Proc. 25th IAEA FEC 2014, San Petersburg, Russia
First author's e-mail address: elena.delaluna@ciemat.es

Abstract. This paper describes experiments recently carried out on JET with the ITER-like wall to investigate the effect of gas fuelling and divertor pumping on high triangularity H-mode plasmas. This paper focused in two main issues: the variation of the global energy confinement with density and the behaviour of edge localized modes (ELMs) at high density. Similar to previously reported observations at low triangularity, operation at $H_{98}=1$ and $\beta_N=2$ can be re-established at high shaping by improved particle control. Though many aspects of high-δ operation were obtained, it was found that H-mode operation was not compatible with high Greenwald fraction, in the range of heating power explored here ($P_{IN}/P_{MARTIN-08} \sim 2$). Interestingly, the usual relationship between type I ELM frequency and density (ELM frequency increasing with density) is not found in high density discharges with high neutral particle content (strong gas puffing and/or reduced pumping). This different behavior reflects the different divertor recycling patterns associated with the change in wall materials.

1. Introduction

The achievement of high confinement at high density is a necessary condition for reaching the ITER target of $Q_{DT}=10$ ($H_{98}=1$, $\beta_N=1.8$ and $n_e/n_{GDL}=0.85$). High performance H-mode operation at high density strongly relies on the improved edge stability provided by higher plasma shaping. In the case of JET with the C-wall, it was found that high confinement quality ($H_{98}=0.9-1$) could be maintained at high density ($n_e/n_{GDL} \geq 0.9$) in highly shaped plasma (with averaged triangularity, $\delta_{av} \geq 0.4$)[1,2]. The good confinement at high density was associated with high pedestal pressure (increase of pedestal density at constant pedestal temperature) and reduced Type I ELM frequency, the so-called 'mixed Type I/II' ELMy regime. The beneficial effect of plasma shaping on confinement has also been reported in JET with the ITER-like wall (ILW), with higher pedestal pressure obtained at higher triangularity in the hybrid scenario (1.4MA/1.7T) at high $\beta_N \sim 2-3$[3]. This behavior, however, was not reproduced in the ELMy H-mode baseline scenario at higher I_p values, where higher gas injection rates ($>10^{22}$ D/s) are typically required to keep W core radiation within acceptable limits. In fact, experiments carried out in JET-ILW in 2012-2014 at high-δ with $I_p=2.5$ MA resulted in a confinement deterioration larger (10-30%) than that observed with the C-wall for similar conditions (I_p, B_t, divertor geometry and gas injection rate) [4]. These experiments showed that increased core shaping enabled higher density H-mode, but the pedestal electron temperature was on average 30–40% lower than in JET-C. Moreover, those earlier experiments at 2.5 MA showed no positive effect of triangularity on global confinement [5]. Only by using nitrogen seeding it was possible to partially recover the confinement at high-δ [4]. The reduced confinement of the high-density H-mode plasmas at high-δ remains one of the least understood results in JET after the change of wall materials. Since a high-δ shape is still the reference shape for ITER, it is important to identify the physics elements that are limiting the pedestal/core confinement of high-δ plasmas in JET-ILW.

Experiments reported in the last IAEA conference showed that divertor geometry strongly affects H-mode plasma performance at low-δ in JET-ILW, with the best confinement obtained when both strike points are located in the divertor corners, where pumping is most efficient [6,7]. Motivated

by these results, a dedicated set of experiments was recently conducted to examine the influence of pumping on confinement, pedestal properties and ELM characteristics of high-δ plasmas in JET-ILW. Only results obtained in unseeded plasmas will be discussed here. The impact of impurity seeding in high-δ plasmas is discussed in a separate paper in this conference [8].

2. Plasma shape and divertor geometry

For the study reported here, high-δ plasmas at 2 MA/2.2 T were run using the four divertor configurations shown in Fig. 1. Averaged triangularity (δ_{av}) varied from 0.36 to 0.39 depending on the divertor target geometry. The names given to the equilibria AA-XY indicate triangularity: low (LT) or high (HT) and target orientation (inner and outer): vertical (V), corner (C) or horizontal (H). For these studies a new high-δ shape (in black in the four panels) was developed with both strikes in the divertor corners (CC), next to the entrance of the pump ducts, enabling effective pumping. The divertor cryopump in JET is located in the sub-divertor structure at the low-field-side (marked with a circle in Fig. 1(a)). Note that earlier high-δ experiments in JET-ILW were carried out in divertor configurations where both strikes points where located far away from the divertor corners, either in the vertical or the horizontal targets (HT-VV and HT-VH configurations in Fig.1). For completeness, a low-δ (δ_{av}=0.22) configuration with both strike points in the divertor corners is also shown. To test the effect of plasma interaction with the top of the machine on confinement at the high-δ, an experiment was performed using the HT-CC configuration where the gap to the top of the machine was increased from 24 cm to 36 cm (separatrix-top real space at R=2.5 m), as seen in Fig. 1(b). Since the change in the top gap did not reveal any variation in global confinement or plasma profiles, the experiment was carried out using the shape with the smaller top gap, allowing the new configuration to be directly compared to the existing high-δ configurations.
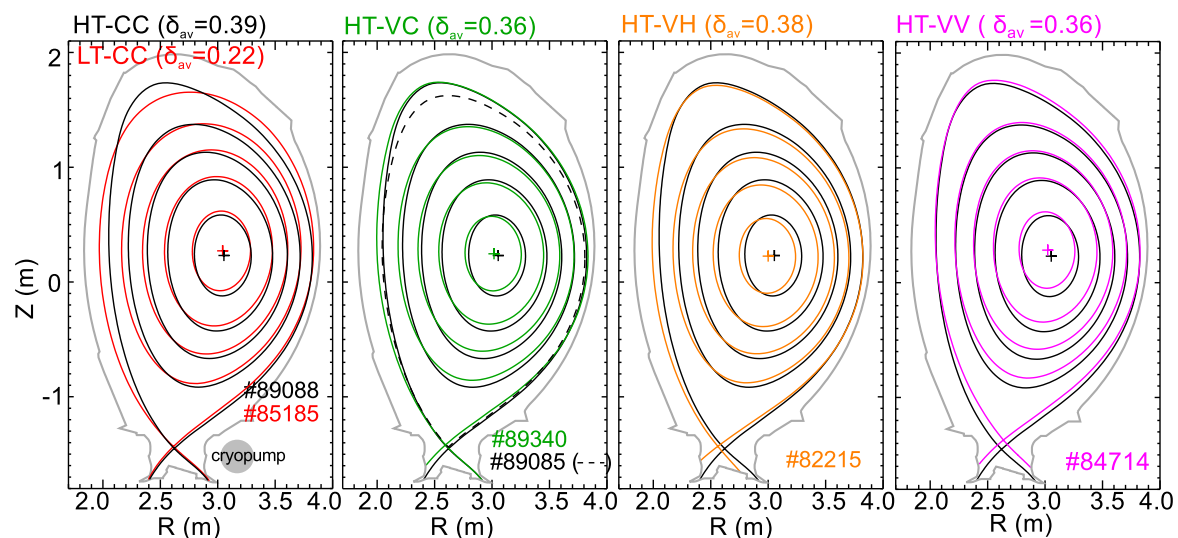

Fig.1. *Plasma shapes at different triangularities and divertor configurations examined in this paper. Configuration names are described in the text. A high-δ shape with larger top clearance is also shown in (b) (dashed line). Approximate location of the cryopump is marked by a circle in (a)*

3. Impact of gas fuelling and divertor geometry on high-δ plasmas

Time traces of selected parameters for three high-δ plasmas showing the impact of gas fuelling and divertor pumping on confinement are compared in Fig. 2, at fixed heating power. The experiment was carried out in steady state conditions and at moderately low heating power (P_{NBI}=12-14 MW, P_{ICRH}=1-2 MW), roughly twice the predicted H-mode threshold power ($P_{MARTIN-08}$). The access to stable conditions against core impurity accumulation set the minimum gas injection rate (Γ_D) used in each configuration, ranging from Γ_D~1.8×10^{22} D/s in the case of the HT-CC configuration to Γ_D~3×10^{22} D/s for the HT-VC configuration. Above this minimum value discharges reach steady conditions, with the stored energy and the line-averaged density
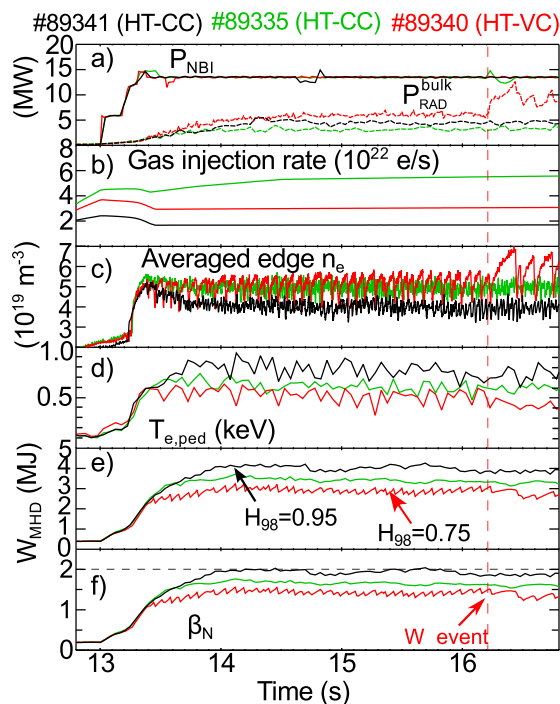
Fig.2. a) NBI and bulk radiated power, b) D gas injection rate, c) averaged edge density d) $T_{e,ped}$ (from TS), e) stored energy and f) normalized beta for three high-δ discharges with different gas and divertor geometry
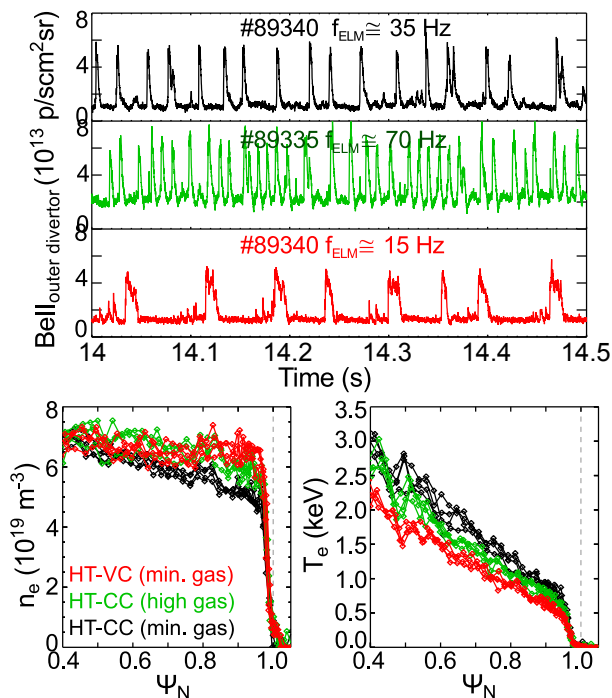

Fig. 3. BeII line emission from the outer divertor (top) and n_e and T_e profiles measured by Thomson Scattering (bottom) just before the ELM crash for the three discharges in Fig.2.

remaining constant for at least 2 seconds (6-10 confinement times) and in most cases for the whole duration of the heating phase (4 s). Similar to previously reported observations at low-δ, the use of the divertor configuration optimized for pumping makes low density operation more accessible also at high-δ, enabling access to higher pedestal temperatures ($T_{e,ped}$) and lower collisionalities. The higher $T_{e,ped}$ achieved in the configuration with optimum pumping, via profile stiffness, leads to an increase of the total plasma pressure (see Fig. 3) and discharges with H_{98}~0.95-1 and β_N~1.8-2 are now routinely obtained at 2 MA at high-δ. No core ion temperatures (T_i) measurements were available in this experiment, but $T_i(0) \approx T_e(0)$ is expected at these high densities. This assumption was confirmed in the pedestal region where $T_{i,ped} \approx T_{e,ped}$ was obtained from edge CXS measurements. Increasing the density with gas puff at fixed configuration (HT-CC in Fig. 2) causes the pedestal to cool down and the confinement degrades, with H_{98} varying from 1 to 0.8 as the density is raised. As seen in Fig. 3 while $n_{e,ped}$ increases monotonically, the central density tends to saturate despite an increasing neutral particle flux. Similar results were obtained with reduced pumping (HT-VC), except that twice as much D gas had to be puffed into the discharge with better pumping to achieve the same edge density. A striking difference is observed, however, in the ELM behavior. We see the usual tendency of the ELM frequency (f_{ELM}) to increase (and the amplitude to decrease) with increasing gas puffing for the HT-CC configuration. In contrast, low frequency (~15 Hz) ELMs with large amplitude develop in the discharge with reduced pumping (#89340 in Fig. 3), producing a strong modulation of the edge n_e (25%) and stored energy (6%).

Fig. 4 summarizes the results of the full gas and divertor geometry scan carried out at high-δ. Here each point represents an averaged value over the steady-state phase of the discharge. In the experiment reported here we chose to focus on the high-δ configuration where pumping is more efficient (HT-CC). A pulse-to pulse gas puff scan was carried out in this case, whereas only data close to the minimum gas injection rate required to access stable conditions was collected for the rest of the divertor configurations. Line-averaged central density increases from 60 to 85% of the Greenwald density limit (n_{GDL}) in the HT-CC gas scan. Similar to observations in JET-C, gas
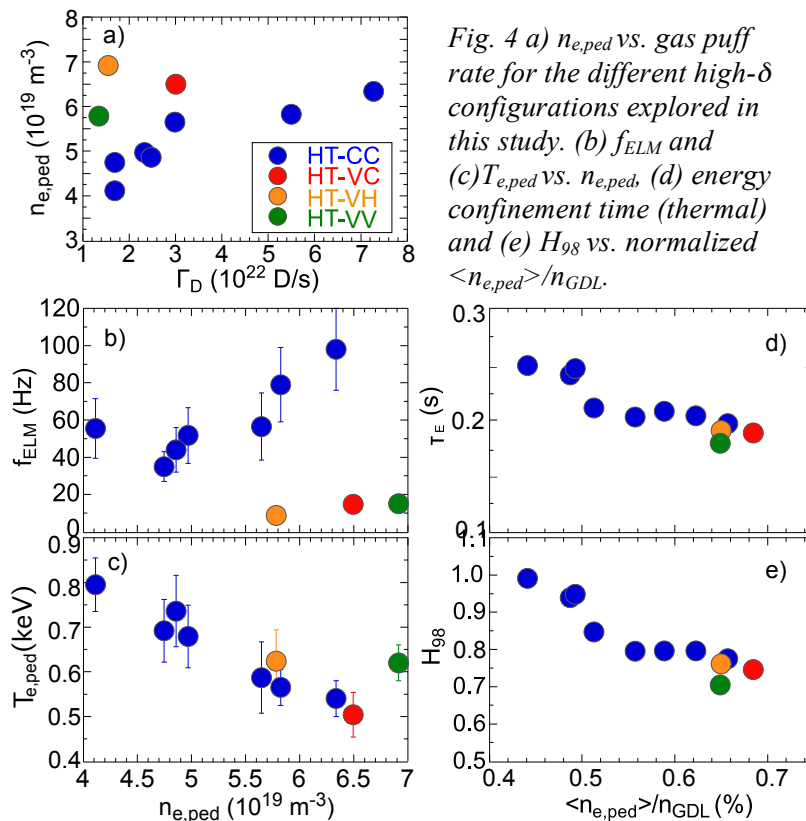
Fig. 4 a) $n_{e,ped}$ vs. gas puff rate for the different high-δ configurations explored in this study. (b) f_{ELM} and (c)$T_{e,ped}$ vs. $n_{e,ped}$, (d) energy confinement time (thermal) and (e) H_{98} vs. normalized $<n_{e,ped}>/n_{GDL}$.

fuelling efficiency rapidly decreases with increasing density. Since effective pumping is only possible through the divertor corners, it is strongly reduced for the configurations VC, VH and VV, resulting in higher densities even at lower gas injection rates. It is worth noting that a reduced pumping is already apparent in the VC configuration, where only the inner strike point is moved away from the inner divertor pump duct. This result is a clear demonstration that the inner divertor is also contributing to the overall pumping. This is supported by evidence from earlier experiments carried out at JET-C with the MkIIGB divertor for which the inner and outer strike points were independently moved in and out from the pump throats [10]. The results of that experiment showed that the inner and outer contribution to pumping were of the same order when the two strike points were located at the same distance from the pump throats. This was attributed to the larger neutral pressure in the inner divertor compared to the outer that promotes better pumping of deuterium and compensates for the different gas conductance in the sub-divertor region between the inner and outer divertor. This asymmetry in the divertor, with the inner divertor denser and colder than the outer divertor, is a typical feature in discharges with forward toroidal magnetic field [11]. As can be seen in Fig. 4, good confinement was achieved only up to a line-averaged pedestal density of 50%n_{GDL} (central density of 70%n_{GDL}). In the optimum pumping case (HT-CC) the effect of gas puffing is to increase f_{ELM} (up to~100 Hz) and reduce $T_{e,ped}$, resulting in a significant (~20%) deterioration of the energy confinement time (thermal stored energy decreases with increasing density) and H_{98} falls from 1 to 0.8. In the absence of a power scan, the classification of the ELMs found at higher densities can not be addressed, but their characteristics (ELM losses, duration time and affected area) are very similar to those found for type I ELMs in JET-C [8]. The density profile remains relatively flat over the entire density range investigated, with no obvious transition to the type III ELM regime, which in JET-C was typically accompanied by a strong collapse of the pedestal density[1]. Confinement remains low (H_{89}<0.8) for all divertor configurations with reduced pumping, in agreement with previous JET-ILW results [4]. Fig. 4 (b) shows the anomalous ELM behaviour found in the discharges with reduced pumping (higher recycling), with f_{ELM} lower (and larger ELMs) at a given density, and for similar $T_{e,ped}$. This finding allows us to conclude that the change in divertor plasma conditions (recycling and radiation), rather than the pedestal collisionality, is the primary factor controlling the appearance of this ELM anomaly. Pedestal collisionality ($\nu_{e,ped}$) in this dataset varies from 0.5 to 1.1, thus plasmas reside in the high collisionality corner of the JET-ILW operational space. No significant differences were found in the achieved confinement or the ELM behaviour between the divertor configurations with reduced pumping, but the limited available data precludes a more comprehensive comparison. The ELM behaviour in high density/high recycling plasmas will be discusses later in the paper.

The dataset shown in Fig. 4 has been compared with 2MA H-mode plasmas at lower triangularity (δ_{av}=0.22) and similar input power (see Fig. 5). At low-δ the gas dose required to maintain stable conditions against W accumulation were smaller (Γ_D=1-1.2×10^{22} D/s) than that used at high-δ, resulting in $f_{ELM}\approx$25-35 Hz. Only one discharge was performed at higher gas puff (3.5×10^{22} D/s). Fig. 5 shows that plasmas with high-δ and efficient pumping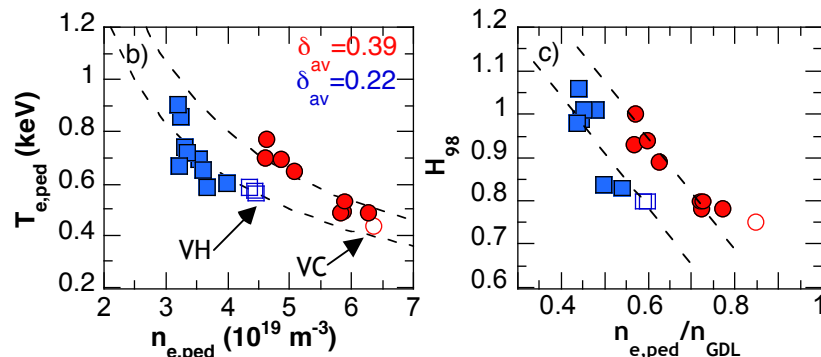 can maintain H-mode with good confinement at higher density than plasmas with lower triangularity. We see that high-δ plasmas display higher pedestal densities and pressures across the density range, resulting in higher $T_{e,ped}$ at the same $n_{e,ped}$. This result is in agreement with peeling-ballooning (P-B) stability predictions and highlights the importance of operating at low collisionality (high edge

Fig. 5. (a) Pedestal n_e-T_e diagram (including lines of constant pressure) and (b) H_{98} confinement factors for low- and high-δ plasmas (2 MA) with optimum (closed symbols) and reduced pumping (open symbols). Dashed lines in (b) are only added to guide the eyes.

bootstrap current) to recover the beneficial effects of triangularity on pedestal stability when approaching the P-B limit. The density peaking vary from 1.3 to 1.5 in the density range shown in Fig. 5, following the usual tendency of decreasing density peaking with increasing pedestal density. As a consequence, the increase in density peaking in the low-δ configuration partly compensates the reduced pedestal pressure, and similar stored energies are obtained at low-δ. As the density is raised by gas fuelling or reduced pumping, $T_{e,ped}$ rapidly decreases, which in turns reduces the edge bootstrap current and the benefits of using a high-δ shape disappear, thus recovering the results of previous studies [5]. As can be seen in the figure, the density range allowing good H-mode confinement (with $H_{98}\geq$0.9) is rather narrow (line-averaged central density between 60% to 70% n_{GDL}), significantly lower than that achieved in JET-C at similar I_p[12].

4. Divertor plasma conditions and relation to ELM dynamics

Inter-ELM divertor plasma conditions have been examined for three discharges from the high-δ density scan (discharges which are similar to those shown in Fig. 2) to determine the role of divertor plasma conditions on the ELM behaviour. In addition to 2-D divertor radiation profiles based on bolometric measurements (Fig. 6), Stark broadening analysis of the high-n Balmer emission lines has been used to measure electron density profiles in the inner divertor region[13]. This is a line-integrated measurement strongly weighted towards the highest emissivity regions along the viewing path with an error of 15%. In all cases, the radiation is greater in the inner
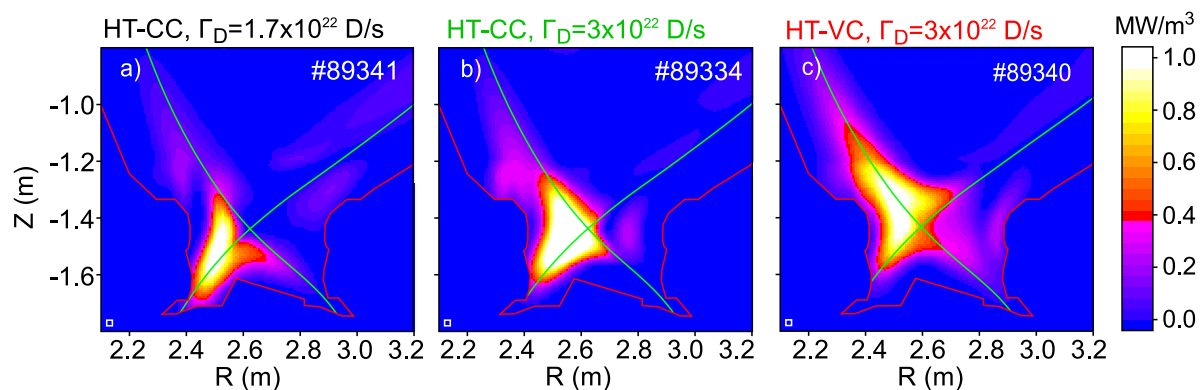

Fig. 6. 2-D bolometric reconstruction of radiated power for #89341 (HT-CC, low gas, f_{ELM}=35 Hz), #89334 (HT-CC, medium gas, f_{ELM} =48 Hz) and #89340 (HT-VC, medium gas, f_{ELM} =15 Hz)
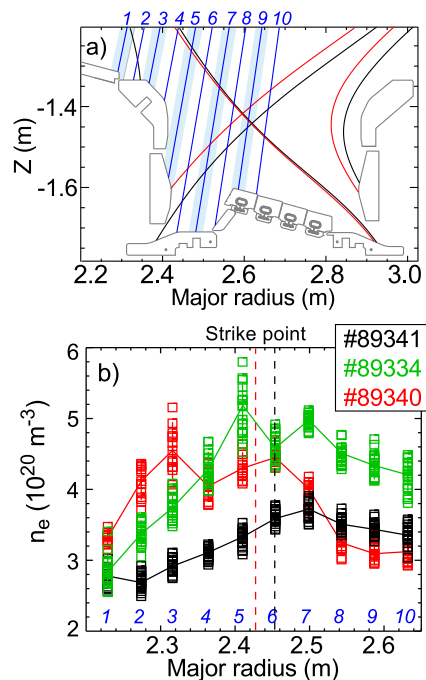
Fig.7. a) Divertor geometry with the spectrometer's line-of-sight for the different channels and b) divertor n_e for the discharges shown in Fig. 6. (channel numbers shown in both figures to guide the eye).

divertor than in the outer. Analysis of the $D\alpha$ and $D\gamma$ signals measured in the inner/outer divertor region are consistent with the inner divertor plasma being partially detached in between ELMs for the discharges with higher Γ_D, whereas the outer divertor plasma remains attached in all three cases. During the ELMs the plasma reattaches briefly, causing the characteristic 'inverted ELM' signature in the inner divertor $D\alpha$ signal. As can be seen in discharges with the divertor corner configuration radiate predominantly along the inner leg, with the region of high radiation expanding towards the high-field-side (HFS) region and the peak radiation moving towards the X-point with increasing gas puff rate. This is consistent with the density profiles shown in Fig. 7. Electron density increases in the inner divertor volume and the peak density moves towards smaller radii with the increase in gas dose, consistent with colder divertor plasma conditions on the HFS. The most dramatic change is observed in the discharge #89340, coincident with the appearance of the large 'slow' ELMs. In this case, with the inner strike point located in the vertical target, the high radiation region spreads over the entire inner divertor and moves upward, away from the target and above the X-point, as a result more power is radiated from the confined region. The formation of this cold and dense region above the divertor baffle on the HFS (HFSHD) is also observed in the inner divertor density profile (peak density found close to channel 3 in Fig. 7(a)). The formation of the HFSHD in high density discharges has been previously reported in AUG and JET-ILW[14].

4. ELM characteristics in high density plasmas

The new experiments at high-δ have shown that ELMs in high density/high recycling H-mode plasmas in JET-ILW do not follow the usual link between ELM losses and pedestal collisionality, with ELM losses decreasing with increasing $\nu_{e,ped}$ [9]. Examination of a more extended dataset (with I_p=1.7–2.5 MA) have shown that the anomalous ELM behavior was also found at high I_p (2.5 MA) in low-δ plasmas, correlated with operation at high density ($n_{e,ped}>5\times10^{19}$ m^{-3}) in conditions of high neutral content resulting from the combined use of high gas injection ($>10^{22}$ D/s) and reduced pumping. This is illustrated in Fig. 8. In this discharge, NBI power was kept constant during the H-mode phase, while the configuration was changed from LT-CC to LT-VH at t=9.58 sec. Owing to the reduced pumping of the VH divertor, pedestal became denser and colder and f_{ELM} was seen to decrease from ~100 Hz to 40 Hz, despite the increase in $\nu_{e,ped}$. The energy loss per ELM (ΔW_{ELM}) in this case increased to values similar to that of ELMs for the same f_{ELM} but at lower $n_{e,ped}$ and higher $T_{e,ped}$. This is different from the type I/type II ELMy regime, where the reduction in f_{ELM} takes place at constant ΔW_{ELM}[1]. A qualitative measure of the increase neutral density is provided by a horizontally viewing $D\alpha$ signal at the plasma midplane; the signal is seen to increase by almost a factor of 2, indicating the strong impact pumping has in the recycling neutral flux. An extreme case in this f_{ELM} anomaly is the development of the large ELMs at $f_{ELM}<15$ Hz seen in the experiment reported here. These type of ELMs were observed in earlier high-δ JET-ILW experiments at 2.5 MA [5] and labeled as 'slow' ELMs because the confinement degradation after the ELM crash last ~10-15 ms, much longer than the ELM enhanced MHD activity (~0.3-0.4 ms in JET-ILW, independent of local pedestal conditions). 'Slow' ELMs have also been found in AUG [15]. A detailed description of the ELM losses for 'slow' and standard ELMs in JET-ILW can be found in [16]. A closer look at the fast pedestal dynamics just after the ELM crash has revealed that the 'slow' ELMs can
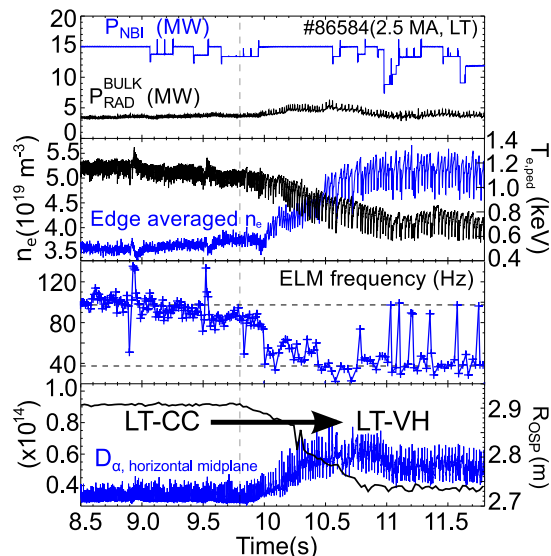
Fig. 8. Relevant time traces for a discharge at low-δ where divertor geometry was changed from CC to VH at 9.58s at fixed heating power. Outer strike position (OSP) movement is shown in the bottom panel.
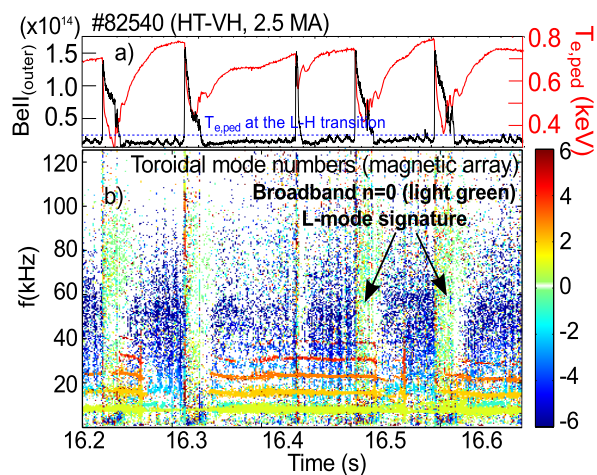

Fig. 9. Spectrum of toroidal mode numbers for a high-δ discharge that exhibit 'slow' ELMs, with a characteristic L-mode feature after the ELM crash. $T_{e,ped}$ and BeII line emission are also shown in (a).

indeed be described as compound ELMs, with short-lived L-mode phases following the ELM crash, during which the confinement is degraded significantly, causing the pedestal recovery to be delayed. This is supported by the analysis of the Mirnov coil signals shown in Fig. 9. An increase of broadband MHD activity with n=0 is clearly seen after the ELM crash in the case of the 'slow' ELMs. This is a usual feature observed in L-mode plasmas. Note that the spectrogram shown in Fig. 9 comprises five ELMs, and only 4 of them fit into the category of compound ELMs described above (note the elevated BeII signal after the ELM crash), showing that both types of ELMs can occur at similar pedestal parameters. We can therefore conclude that the development of the second phase in the ELM dynamics must be unrelated to the MHD instability that triggers the ELM. We found out that, in addition to high density/recycling conditions, low $T_{e,ped}$ was necessary for the development of the large compound ELMs. The lower $T_{e,ped}$, the smaller the margin between the lower end of the ELM cycle and the critical temperature for the transition to L-mode. This explains why the ELMs are compound in #82540 (Fig. 9) but not in the high density/high recycling phase in #86584 (Fig. 8).

From the available experiments it is clear that the changes in divertor plasma conditions, rather than in pedestal top parameters, are the dominant factor in observed changes in ELM behaviour, but the physics which determines those changes is still unclear. ELM dynamics can be modified by changes in the edge stability and/or in the edge transport (affecting inter-ELM pedestal evolution). It should be noted that the pressure pedestal in high-gas experiments (as it is the case in the one reported here) are usually found to be deeply stable to P-B instabilities [17]. Preliminary analysis has found that the relative radial shift (Δr_{ped}) between the n_e and T_e pedestal position increased (from 1.4 to 1.8% of poloidal flux) with increasing density. These results are in fair agreement with a recent study carried out in JET-ILW for a low-δ dataset[18], where an increase in the relative shift was linked (via its effect on pedestal stability) to confinement deterioration. Analysis is ongoing to evaluate the influence of this effect in the case of the high-δ plasmas, obtained at lower input power and higher gas injection rates than the low-δ discharges analysed in [18]. On the other hand, detachment of the divertor and movement of the radiation to the X-point might affect edge transport degrading the confinement, either by edge cooling inside the separatrix or by penetration of neutrals towards the core (very small effect as shown in [7]). SOL physics might also be involved. Measurements of the upstream density profiles show an increase in the electron density in the vicinity of the separatrix and in the far SOL as the pedestal density rises. Such changes could alter both the pedestal stability and possibly the edge transport. Moreover, it is argued in [19] that a complex interplay between implantation, desorption and

recycling of deuterium on the W target plates after the ELM heat pulse might affect the density pedestal build up after the ELM crash. Further experimental and modelling studies are required to evaluate in detail the influence of the different mechanisms on the observed ELM behaviour.

5. Conclusions

The new experiments reported here have shown that H-mode operation at H_{98}=1 and β_N=1.8-2 can be re-established at high shaping (up to 2 MA so far) in the baseline scenario on JET-ILW by improved particle control. Optimum pumping appears to be a key element to access to good confinement in the baseline scenario at high-δ where high gas injection rates ($>10^{22}$ D/s) are required to avoid core W accumulation, confirming the earlier experiments at low-δ. Though many aspects of high-δ operation were obtained, it was found that H-mode operation was not compatible with high density and high Greenwald fraction, in the range of heating power explored here ($P_{IN}/P_{MARTIN-08}\sim2$). Maintaining a robust pedestal (high $T_{e,ped}$) is a key element in the access to good confinement conditions at high density for high-δ H-mode plasmas, since it holds the edge bootstrap current at a level needed to access the improved edge stability provided by increased triangularity. This was not the case in JET-ILW experiment, where the edge rapidly cooled down as the density increased with gas fuelling, resulting in the loss of the H-mode confinement at lower densities than those obtained in JET-C. Physics understanding of the mechanisms involved in the strong energy confinement degradation seen in JET-ILW at high density is key to allow extrapolation to ITER. The higher recycling conditions (high gas injection and/or reduced pumping) present in the JET-ILW baseline H-mode scenario is the most likely candidate to explain the differences found in JET-C and JET-ILW at high density, but the mechanisms responsible of these differences are still poorly understood. No attempt has been made yet to overcome the limit encountered in this experiment. Following the P-B stability model, a possible option would be to perform the gas scan at higher heating power, thus enabling operation at higher $T_{e,ped}$ (lower collisionality) and higher β_N. Both mechanisms tend to facilitate the access to the region of pedestal stability diagram where strong shaping is the most effective at improving stability, which in turn may modify the subsequent n-T trajectory during a density scan. This will be the subject of future experiments in JET-ILW. The new experiments at high-δ have provided convincing experimental evidence that higher recycling (high gas and lack of pumping) in JET-ILW affected not only the pedestal parameters but also the ELM dynamics. A significant progress has been made in identifying the key parameters responsible of the different ELM phenomenology encountered in high density H-mode plasmas in JET-ILW, but it remains to be understood which are the dominant physics process involved in the observed ELM behaviour.

References

[1] G. Saibene et al, Plasma Phys. Control. Fusion **44** (2002) 1769
[2] C. Giroud et al, Nuclear Fusion **52** (2012) 063022
[3] C. Challis et al, Nuclear Fusion **55** (2015) 053031
[4] C. Giroud et al, Nuclear Fusion **53** (2013) 113025
[5] M. Beurskens et al, Nuclear Fusion **54** (2014) 043001
[6] E. de la Luna et al, (EX/P5-29) 25th IAEA Fusion Energy Conf. (Saint Petersburg, Russia, 2014)
[7] P. Tamain et al, (2015) Journal Nuclear Materials **463** (2015) 450
[8] C. Giroud et al, this conference
[9] A. Loarte et al, Plasma Phys. Control. Fusion **44** (2002) 1815
[10] E. Tsitrone et al, Plasma Phys. Control. Fusion **44** (2002) 701

[11] A. Loarte et al, Plasma Phys. Control. Fusion **43** (2001) R183
[12] R. Sartori *et al, Plasma Phys. Control. Fusion* **44** (2002) 1801
[13] B. Lomanowski et al, Nuclear Fusion **55** (2015) 123028
[14] S. Potzel et al, Journal of Nucl. Materials **463** (2015) 541
[15] P. Schneider et al, Plasma Phys. Control. Fusion **56** (2014) 025011
[16] L. Frassinetti et al, Nuclear Fusion **55** (2015) 023007
[17] C. Maggi et al., Nuclear Fusion **55** (2015) 113031
[18] E. Stefanikova et al, 43rd EPS 2016
[19] S. Brezinsek et al., Phys. Scr. (2016) 01407